View metadata, citation and similar papers at core.ac.uk
brought to you by CORE
provided by Repository@USM

SYNTHESIS AND ACTIVITY STUDIES OF NOVEL DISPIRO PYRROLIDINE COMPOUNDS AS POTENTIAL ANTIMYCOBACTERIAL AGENTS

ANG CHEE WEI

UNIVERSITI SAINS MALAYSIA

2015

SYNTHESIS AND ACTIVITY STUDIES OF NOVEL DISPIRO PYRROLIDINE COMPOUNDS AS POTENTIAL ANTIMYCOBACTERIAL AGENTS

by

ANG CHEE WEI

Thesis submitted in fulfillment of the requirements

for the Degree of

Master of Science

November 2015

ACKNOWLEDGEMENTS

During my MSc course, I have been surrounded by many great people who have given me their support physically and morally. Foremost, I would like to express my sincere gratitude to my supervisor Prof. Tan Soo Choon, for his patience and motivation, not to mention providing me an excellent atmosphere in doing research. His guidance and supervision in my graduate education proved to be priceless. I would not be able to finish this dissertation without his persistent help. A deep appreciation also goes to my co-supervisor, Prof. Rusli Ismail, for his inspiration and support.

I owe my gratitude to Dr. Mohamed Ashraf Ali, for being a superb mentor to me. He has opened up my eyes in the field of drug discovery and his deep insights have shaped the essential part of this work. I would like to thank Dr. Choi Sy Bing and Dr. Vijay Masand for helping me to develop my background in molecular docking. I am grateful to Dr. Oon Chern Ein for her patience and guidance in cell culture work. I also appreciate the help of Prof. Hasnah Osman and her research group for recording the 1D and 2D NMR spectra.

In addition, I would like to take this opportunity to thank National Institute of Health and the National Institute of Allergy and Infectious Diseases, USA for screening of my compounds against *Mycobacterium tuberculosis*. I wish to acknowledge the School of Chemical Sciences, USM and Usains Biomics Sdn Bhd, for providing the facilities and training in operating the analytical instruments. Special thanks go to my fellow colleagues from Prof. Tan’s group for the stimulating discussions and endless support throughout these years.

I extend my warmest appreciation to my family, for all they have done for me since I was born. They always stand by me whenever I need a rest. Never forget to thank my best research partner and soul mate, Yeong Keng Yoon, for the unconditional support and confidence given to me in starting this research journey. I am lucky enough to have him travelling the same route with me.

Finally, I dedicate this dissertation to the memory of my beloved father and grandparents, who are my source of inspiration and motivation forever.

TABLE OF CONTENTS

PAGE

ACKNOWLEDGEMENTS **ii**

TABLE OF CONTENTS **iv**

LIST OF TABLES **x**

LIST OF FIGURES **xii**

LIST OF ABBREVIATIONS **xxii**

ABSTRAK **xxvii**

ABSTRACT **xxix**

CHAPTER ONE **1**

INTRODUCTION **1**

1.1 Tuberculosis 1

1.1.1 Overview 1

1.1.2 *Mycobacterium tuberculosis* 2

1.1.3 Current TB drug therapy 3

1.1.3(a) First-line TB drugs 4

(i) Isoniazid (INH) 4

(ii) Rifampicin (RIF) 5

(iii) Pyrazinamide (PZA) 6

(iv) Ethambutol (EMB) 7

1.1.3(b) Second-line TB drugs 8

1.1.4 Challenges in TB treatment 9

1.1.5 New drugs in pipeline 10

1.1.6 Potential drug targets 13

1.2 Drug design 16

1.2.1 Overview 16

1.2.2 Green chemistry in drug discovery 19

1.2.3 1,3-dipolar cycloaddition 21

1.2.4 Molecular docking in drug design 24

1.3 Heterocyclic compounds in Drug Discovery 26

1.3.1 Overview 26

1.3.2 Spiro compounds 28

1.3.3 Indanones 30

1.3.4 Pyrrolidine 32

1.4 Research objectives 34

CHAPTER TWO 35

SYNTHESIS OF DISPIRO PYRROLIDINES USING 1,3-DIPOLAR CYCLOADDITION 35

2.1 Introduction 35

2.2 Aim of experiment 36

2.3 Materials 36

2.4 Instrumentation 38

2.5 Methods 38

2.5.1 Synthesis of 2-[(*E*)-1-(Substituted aryl) methylidene]-1-indanone (**1a-1m**) 38

2.5.1(a) Conventional stirring method at room temperature 38

2.5.1(b) Grinding method using pestle and mortar 40

2.5.2 Synthesis of substituted aryl-1´-methyldispiro[indan-2,2′ pyrrolidine-3′,2″-indan]-1,3,1″-trione analogues (**2a-2m**) 40
2.5.3 Synthesis of substituted aryl-1′-methyldispiro[acenaphthylene-1,2′ pyrrolidine-3′,2″-indan]-2,1″(1*H*)-dione analogues (**3a-3m**) 41
2.5.4 Synthesis of substituted 7′-aryl-5′,6′,7′,7a′-tetrahydrodispiro[indan-2,5′-pyrrolo[1,2-*c*][1,3]thiazole-6′,2″-indan]-1,3,1″-trione analogues (**4a-4m**) 42
2.5.5 Synthesis of substituted 7′-aryl-1′,3′,5′,6′,7′,7a′-hexahydrodipiro [acenaphthylene-1,5′-pyrrolo[1,2-*c*]thiazole-6′,2″-indane]-2,1″(1H)-dione analogues (**5a-5m**) 43
2.6 Results and discussion 44
2.6.1 Mechanism of reaction 44
2.6.1(a) Claisen-Schmidt condensation 44
2.6.1(b) 1,3-dipolar cycloaddition 45
2.6.2 Parameters in 1,3-dipolar cycloaddition 49
2.6.3 Physical characterization 52
2.7 Conclusion 82
CHAPTER THREE **83**
CELL BASED AND ENZYMATIC STUDIES OF MYCOBACTERIUM TUBERCULOSIS **83**

3.1 Introduction 83

3.2 Aim of experiment 85

3.3 Materials 86

3.4 Methods 87

3.4.1 Bacterial culture 87

3.4.2 Preparation of compound libraries 88

3.4.3 Mycobacterium tuberculosis dose response assay 88

3.4.4 Analysis of dose response data 90

3.4.5 Cytotoxicity test 90

3.4.6 Fluorescence quenching analysis 91

3.5 Results and discussion 92

3.5.1 Antimycobacterial activity 92

3.5.2 Structure-activity relationship (SAR) 102

3.5.2(a) Changes of substituents at site **I** 102

3.5.2(b) Replacement at site **II** and **III** 104

3.5.3 Cytotoxicity studies on Hs27 and primary colorectal fibroblasts 107

3.5.4 Fluorescence quenching effect on InhA 108

3.6 Conclusion 114

CHAPTER FOUR 115

MOLECULAR DOCKING STUDY 115

4.1 Introduction 115

4.2 Aim of experiment 117

4.3 Methods 117

4.3.1 Docking tools 117

4.3.2 Molecular docking procedure 117

4.3.2(a) Protein structure preparation 118

4.3.2(b) Ligand preparation 119

4.3.2(c) Receptor grid generation 119

4.3.2(d) Ligand docking 119

4.3.3 ADME prediction 120

4.3.4 Solubility analysis 120

4.4 Results and discussion 121

4.4.1 Analysis of InhA binding site 121

4.4.2 Validation of docking protocol using Glide 123

4.4.3 Docked conformations of lead compound 124

4.4.4 SAR study using molecular docking 130

4.4.4(a) Comparison of docking poses of derivatives from the same series (site **I**) 130

4.4.4(b) Comparison of docking poses of derivatives from other series (site **II** and 134

4.4.5 ADME-related physiochemical properties 140

4.4.6 Aqueous solubility of the lead compound 142

4.5 Conclusion 143

CHAPTER FIVE **144**

GENERAL DISCUSSION AND CONCLUSION **144**

5.1 General discussion 144

5.2 Conclusion 148

5.3 Future perspectives 149

REFERENCES **151**

APPENDICES **172**

Appendix A 172

Appendix B 176

Appendix C 180

LIST OF PUBLICATIONS **186**

LIST OT TABLES

Page

Table 2.1 The amounts of various aromatic aldehydes (equivalent to 1 mmol) used in syntheses of **1a-1m**. 39

Table 2.2 Yield of isolated product of compound **2a** (as representative) after reflux for 6 hours using different solvents. 50

Table 2.3 Percentage of yields, CHN microanalytical data and R_f values of compounds **2a-2m**. 53

Table 2.4 Percentage of yields, CHN microanalytical data and R_f values of compounds **3a-3m**. 54

Table 2.5 Percentage of yields, CHN microanalytical data and R_f values of compounds **4a-4m**. 55

Table 2.6 Percentage of yields, CHN microanalytical data and R_f values of compounds **5a-5m**. 56

Table 2.7 Melting points of compounds with crystal structure. 57

Table 2.8 ^{1}H-^{1}H correlations as inferred from the 2D COSY for compound **3c**. 59

Table 2.9 ^{1}H-^{13}C correlations as inferred from the 2D HMQC and HMBC for compound **3c**. 63

Table 3.1 Antimycobacterial activity of dispiro pyrrolidine derivatives **2a-m**. 98

Table 3.2 Antimycobacterial activity of dispiro pyrrolidine derivatives **3a-m**. 99

Table 3.3 Antimycobacterial activity of dispiro pyrrolidine derivatives **4a-m**. 100

Table 3.4 Antimycobacterial activity of dispiro pyrrolidine derivatives **5a-m**. 101

Table 3.5 Selectivity index values of the potent compounds **3b**, **3c** and **3d**. 108

Table 4.1 Binding interaction data of **3c** with the important residues in active site of InhA . 129

Table 4.2 Comparison of hydrophobic contacts between the substrate and **3c** in the binding pocket. 130

Table 4.3 Results of docking study of the selected compounds as compared with their antimycobacterial activity. 140

Table 4.4 Predicted ADME-related physicochemical parameters of top three most potent compounds. 141

Table B.1 Selected ^{1}H NMR chemical shifts (δ in ppm) and coupling constants (J in Hz) of compounds from series **2**. 176

Table B.2 Selected ^{1}H NMR chemical shifts (δ in ppm) and coupling constants (J in Hz) of compounds from series **3**. 177

Table B.3 Selected ^{1}H NMR chemical shifts (δ in ppm) and coupling constants (J in Hz) of compounds from series **4**. 178

Table B.4 Selected ^{1}H NMR chemical shifts (δ in ppm) and coupling constants (J in Hz) of compounds from series **5**. 179

Table C.1 Mass recorded using electronspray ionization mass spectrometry (ESI-MS) in positive ion mode. 184

LIST OT FIGURES

Page

Figure 1.1 Scanning electron micrograph of *Mycobacterium tuberculosis* ranges in length between 2 - 4 microns, and a width between 0.2 - 0.5 microns (Adapted from Butler, 2006). 3

Figure 1.2 Chemical structure of isoniazid. 5

Figure 1.3 Chemical structure of rifampicin. 6

Figure 1.4 Chemical structure of pyrazinamide. 7

Figure 1.5 Chemical structure of ethambutol. 8

Figure 1.6 Structures of some second-line drugs for TB treatment. 9

Figure 1.7 Chemical structures of potential TB drugs in clinical development. 12

Figure 1.8 Newly approved drugs for treatment of MDR-TB under “interim policy guideline”. 13

Figure 1.9 Targets implicated in TB disease (Adapted from Lamichhane, 2011). 14

Figure 1.10 FAS II system in *Mycobacterium tuberculosis*. 15

Figure 1.11 Activation of isoniazid (INH) by KatG to form INH-NAD adduct that inhibits InhA enzyme. 16

Figure 1.12 Process of drug discovery and development (Modified from *Nature Reviews Drug Discovery* (Wenk, 2005, Cooper, 2002)). 17

Figure 1.13 Synthesis of ibuprofen by using conventional six-step method (A) and the green synthesis that was reduced to three steps (B). 20

Figure 1.14 General scheme of 1,3-dipolar cycloaddition. 22

Figure 1.15 Examples of 1,3-dipolar cycloadditions in constructing various types of 5-membered heterocyclic compounds. 23

Figure 1.16 Known synthetic routes of different cycloadducts that have been published previously (Fokas et al, 1998; Dürüst et al., 2011; Xiao et al.). 24

Figure 1.17 Novel InhA inhibitors that were identified through pharmacophore modelling and virtual screening using four docking programs. 25

Figure 1.18 Structures of some natural and synthetic heterocyclic drugs. 27

Figure 1.19 Examples of chemical structures with monospiro, dispiro and trispiro ring systems. 28

Figure 1.20 Structure of (-)-perhydrohistrionicotoxin with a chiral spiro centre. 29

Figure 1.21 Pd (II)-catalyzed dehydrative cyclization of ketoallylic diols to form spiroketals under mild conditions (Palmes et al., 2013). 29

Figure 1.22 Williams' 1,3-dipolar cycloaddition approach to synthesize spirotryprostatin B (Sebahar and Williams, 2000). 30

Figure 1.23 Structures of (A) 1-indanone with its active centers; (B) 2-indanone (Özkilinç, 2009). 31

Figure 1.24 Examples of some bioactive indanone derivatives. Rings coloured in red are core structure of indanones. 31

Figure 1.25 Structures of several naturally occurring pyrrolidine alkaloids. 32

Figure 1.26 Examples of spiropyrrolidinyl alkaloids with potential biological activities. 33

Figure 1.27 Mechanism of formation of spiro-oxindole pyrrolidine through 1,3-dipolar cycloaddition (Li et al., 2014). 33

Figure 2.1 Claisen-Schmidt condensation reaction between 1-indanone and different types of aromatic aldehydes (represented by R) to produce 2-[(*E*)-1-(substituted aryl) methylidene]-1-indanone **(1a-1m)**. 40

Figure 2.2 Reaction of substituted indanone, ninhydrin and sarcosine to form aryl-1´-methyldispiro[indan-2,2′ pyrrolidine-3′,2″-indan]-1,3,1″-trione analogues (**2a**-**2m**). 41

Figure 2.3 Reaction of substituted indanone, acenaphthenequinone and sarcosine to form aryl-1′-methyldispiro[acenaphthylene-1,2′ pyrrolidine-3′,2″-indan]-2,1″(1*H*)-dione analogues (**3a**-**3m**). 42

Figure 2.4 Reaction of substituted indanone, ninhydrin and thiazolidine-4-carboxylic acid to form substituted 7′-aryl-5′,6′,7′,7a′-tetrahydrodispiro[indan-2,5′-pyrrolo[1,2-*c*][1,3]thiazole-6′,2″-indan]-1,3,1″-trione analogues (**4a-4m**). 43

Figure 2.5 Reaction of substituted indanone, acenaphthenequinone and thiazolidine-4-carboxylic acid to form substituted 7′-aryl-1′,3′,5′,6′,7′,7a′-hexahydrodipiro[acenaphthylene-1,5′-pyrrolo[1,2-*c*]thiazole-6′,2″-indane]-2,1″(1H)-dione analogues (**5a-5m**). 44

Figure 2.6 Mechanism of Claisen-Schmidt condensation. 45

Figure 2.7 Mechanism for the formation of azomethine ylides using (A) ninhydrin and sarcosine; (B) acenaphthenequinone and sarcosine; (C) sarcosine and thiazolidine-4-carboxylic acid; and (D) acenaphthenequinone and thiazolidine-4-carboxylic acid. 47

Figure 2.8 Mechanism for the regioselective formation of dispiro pyrrolidine using indanone derivatives, acenaphthenequinone and sarcosine. 48

Figure 2.9 Regioselective cycloaddition of compound **3c**. SOI represents the secondary orbital interaction between the carbonyl group of dipolarophile with those of azomethine ylide. 49

Figure 2.10 Effect of varying the amount of sarcosine (per mmol of indanone and ninhydrin) on the yield of product, **2a**. 51

Figure 2.11 Effect of varying the amount of ninhydrin on the yield of product, **2a**. 51

Figure 2.12 Structure of compound **3c** with complete atomic numbering. 58

Figure 2.13 Selected HMBC correlations of compound **3c**. 62

Figure 2.14 ^{1}H NMR spectrum of the representative compound, 4´-(4-bromophenyl)-1´-methyldispiro[acenaphthylene-1,2´-pyrrolidine-3´,2″-indane]-2,1″(1*H*)-dione (**3c**). 64

Figure 2.15 ^{13}C NMR spectrum of the representative compound **3c** dissolved in $CDCl_3$. 65

Figure 2.16 DEPT-135 spectrum of compound **3c**. 66

Figure 2.17 ^{1}H-^{1}H COSY spectrum of compound **3c**. 67

Figure 2.18 ^{1}H-^{13}C HMQC spectrum of compound **3c**. 68

Figure 2.19 ^{1}H-^{13}C HMBC spectrum of compound **3c**. 69

Figure 2.20 Structure of compound **2d** with complete atomic numbering and its selected ^{1}H and ^{13}C NMR chemical shifts. 70

Figure 2.21 ^{1}H NMR spectrum of **2d**, representative compound from series **2**, in $CDCl_3$. 71

Figure 2.22 ^{13}C NMR spectrum of **2d** in $CDCl_3$. 72

Figure 2.23 Structure of compound **4b** with complete atomic numbering and its selected ^{1}H and ^{13}C NMR chemical shifts. 73

Figure 2.24 ^{1}H NMR spectrum of **4b**, representative compound from series **4**, in $CDCl_3$. 74

Figure 2.25 ^{13}C NMR spectrum of **4b** in $CDCl_3$. 75

Figure 2.26 Structure of compound **5c** with complete atomic numbering and its selected ^{1}H and ^{13}C NMR chemical shifts. 76

Figure 2.27 ^{1}H NMR spectrum of **5c**, representative compound from series **5**, in $CDCl_3$. 77

Figure 2.28 ^{13}C NMR spectrum of **5c** in $CDCl_3$. 78

Figure 2.29 Mass spectrum of **3c** in positive ion mode. 80

Figure 2.30 ORTEP diagram of compound **3c**. Weak hydrogen bonds are indicated by dashed lines. 81

Figure 3.1 Schematic of the 384-well plate for dose response studies. 89

Figure 3.2 Chemical reaction of luciferin, ATP, oxygen and Mg^{2+} catalysed by the recombinant firefly luciferase (Adapted from Promega Technical Bulletin, 2012). 92

Figure 3.3 Number of active compounds in each series as evaluated from their IC_{50} and MIC values. Compounds with IC_{50} and MIC of less than or equal to 100 µM were considered to be active. 94

Figure 3.4 Substituents at different sites **I**, **II** and **III** in compound from series **3**. 94

Figure 3.5 Dose response curve of compound **3c** against Mycobacterium tuberculosis $H_{37}R_V$ strains as compared with the standard drugs (isoniazid, ethambutol, cycloserine and pyrimethamine). Red lines indicated the concentrations needed to inhibit 50% of the bacteria growth; outliers were eliminated from curve fitting. 95

Figure 3.6 Structures of the top four most potent compounds, **3c**, **3d, 3b** and **3e**. 96

Figure 3.7 Dose-response curve of compounds **3b**, **3d** and **3e**. Red lines indicated the concentrations needed to inhibit 50% of the bacteria growth; outliers were eliminated from curve fitting. 97

Figure 3.8 IC_{50} comparisons of compounds containing halogen substituent from series **3**. 103

Figure 3.9 Structural differences of compounds from series **3** and **5** at site **II** and their dose response curves. (A) Derivatives with electron withdrawing group (chloro). (B) Derivatives with electron donating group (methoxy). 105

Figure 3.10 IC_{50} comparison charts of compounds from series **2** and **3**. 106

Figure 3.11 IC_{50} comparison charts of compounds from series **4** and **5**. 106

Figure 3.12 Cytotoxicity assay results for the actives **3b**, **3c** and **3d** at six different concentrations range from 2.5 to 250 µM (2.5, 10, 25, 50, 125, 250 µM). 107

Figure 3.13 Emission spectrum and fluorescence intensity of InhA in complex with triclosan, compound **3c** and ciprofloxacin at a fixed concentration of 100 µM after incubating with 2 µM of InhA for 30 minutes. 110

Figure 3.14 Emission spectrum of InhA in complex with triclosan (A) and compound **3c** (B) using different concentrations. 111

Figure 3.15 (A) Relative fluorescence quenching intensity (FQ) of InhA upon binding to triclosan and compound **3c** at various concentrations. (B) The changes of fluorescence intensity (F_0-F) against triclosan and **3c**. The hyperbolas indicate the best fit of the data. 112

Figure 3.16 Time-dependent binding of **3c** to 2 µM of InhA within a time frame of 30 min. 113

Figure 4.1 Flow chart of the simplified methodology used for protein-ligand docking in this study. 118

Figure 4.2 Structure of the native ligand, 1-cyclohexyl-N-(3,5-dichlorophenyl)-5-oxopyrrolidine-3-carboxamide in the protein crystal structure. 122

Figure 4.3 Ribbon presentation of *M. tuberculosis* enoyl-acyl carrier protein reductase, InhA (PDB ID: 4TZK). The cofactor, NAD is in red tubes whereas the bound ligand, 1-cyclohexyl-N-(3,5-dichlorophenyl)-5-oxopyrrolidine-3-carboxamide is in green tubes. 122

Figure 4.4 Overlays of native ligand in the crystal structure before (green) and after dock (black). Both structures are overlapped with each other, which correlates with the low RMSD value (0.238 Å). 123

Figure 4.5 Docked conformation of lead compound **3c** (purple) superimposed with the bound ligand (black) in the active site. The substrate-binding loop of InhA (residues 196-219) is represented in blue cartoon. 124

Figure 4.6 Comparison of the binding pockets. (A) The surface presentation of NADH and *trans*-2-hexadecanoyl-*N*-acetyl cysteamine thioester substrate binding site (PDB code: 1BVR); (B) Superposition of various InhA inhibitor such as *N*-(4-metylbenzoyl)-4-benzylpiperidine (blue, PDB code: 2NSD), 5-(4-(9H-fluoren-9-yl)piperazin-1-yl)carbonyl-1H-indole (red, PDB code: 1P44) and *N*-(5-chloro-2-methylphenyl)-1-cyclohexyl-5-oxopyrrolidine-3-carboxamide (green, PDB code: 4UOK); (C) Superposition of the lead compound **3c** (purple) in the same substrate binding pocket as most of the inhibitors. 125

Figure 4.7 Hydrogen bonding network of compound **3c** with the catalytic residue, Tyr 158 and cofactor, NAD+ in InhA. 126

Figure 4.8 Binding interactions of compound **3c** with InhA. Panel (A) shows residues that have potential to form halogen bonds with the important residues within 4.0 Å of Br substituent. Panel (B) represents π-π stacking formed between 4′-phenyl moiety and Tyr 158. Panel (C) displays protein-ligand interactions of **3c** with the hydrophobic residues (green) at the active site. 128

Figure 4.9 Overlay of **3b** (blue) with **3c** (purple) in the active site. 131

Figure 4.10 (A) Structural difference between compound **3c** and **3f** at site **I**. (B) Superposition of docked conformation of **3f** (red) and **3c** (purple) in the binding pocket. 132

Figure 4.11 3D structure of **3j** and its **s**elected interactions with the important residues near the substrate binding loop (represented in blue cartoon). Dashed line indicates the hydrogen bond that formed between ligand and catalytic residue, Tyr 158. 133

Figure 4.12 3D structure of **3g** (left) and its interactions with the key residues in the active site. Dashed line indicated the hydrogen bond between **3g** and Gly 96. 134

Figure 4.13 Structural difference between compound **3c** and **5c**. 135

Figure 4.14 Best pose of **3c** (top) and **5c** (bottom) at the active site. The substituents at pyrrolidine ring were surrounded by the catalytic triad, Phe 149-Tyr 158-Lys 165. 135

Figure 4.15 Structural differences between compound **3c** and **2c**. 136

Figure 4.16 Best pose of **3c** (top) and **2c** (bottom) at the active site. White dashed lines indicate the hydrogen bonding; residues shown in green formed hydrophobic contacts with the acenaphthyleneone/ninhydrin ring at site **III**. 137

Figure 4.17 (A) 2D structure of compound **4c**. (B) Overlay of **4c** with **3c** in the active site, with their structural differences highlighted using red boxes. 138

Figure 4.18 Hydrogen bondings (white dashed lines) were formed between **4c** and Tyr 158 (1.90 Å) and NAD+ (2.33 Å). π-π stacking between 4´-phenyl and aromatic Tyr 158 was displayed in blue dashed lines. 138

Figure 4.19 Rationale in designing lead compound against InhA. 139

Figure 4.20 UV spectrum of compound **3c** in acetonitrile, with λ_{max} at 318 nm. 142

Figure 4.21 Calibration curve of **3c** in a range of 0.3125-100 µM. 143

Figure A.1 Structures of substituted aryl-1´-methyldispiro[indan-2,2′ pyrrolidine-3′,2″-indan]-1,3,1″-trione analogues (**2a-2m**) from series **2**. 172

Figure A.2 Structures of substituted aryl-1′-methyldispiro[acenaphthylene-1,2′ pyrrolidine-3′,2″-indan]-2,1″(1*H*)-dione analogues (**3a-3m**) from series **3**. 173

Figure A.3 Structures of substituted 7′-aryl-5′,6′,7′,7a′-tetrahydrodispiro[indan-2,5′-pyrrolo[1,2-*c*][1,3]thiazole-6′,2″-indan]-1,3,1″-trione analogues (**4a-4m**) from series **4**. 174

Figure A.4 Structures of substituted 7′-aryl-1′,3′,5′,6′,7′,7a′-hexahydrodipiro[acenaphthylene-1,5′-pyrrolo[1,2-c]thiazole-6′,2″-indane]-2,1″(1H)-dione analogues (**5a-5m**) from series 4. 175

Figure C.1 Mass spectrum of representative compound, **2d** from series **2** in positive ion mode. 180

Figure C.2 Mass spectrum of representative compound, **3g** from series **3** in positive ion mode. 181

Figure C.3 Mass spectrum of representative compound, **4f** from series **4** in positive ion mode. 182

Figure C.4 Mass spectrum of representative compound, **5j** from series **5** in positive ion mode 183

LIST OF ABBREVIATIONS

%	Percent
ºC	Degree Celsius
Å	Angstrom
δ	Delta, chemical shift scale
µL	Microliter
µm	Micrometer
λ_{max}	Wavelength of maximum absorption
α	Alpha
β	Beta
1D	One-dimensional
2D	Two-dimensional
3D	Three-dimensional
AB	AlamarBlue
ACP	Acyl carrier protein
ADC	Albumin, dextrose, catalase
ADME	Absorption, distribution, metabolism and excretion
ATCC	American Type Culture Collection
AMP	Adenosine monophosphate
ATP	Adenosine triphosphate
^{13}C NMR	Carbon nuclear magnetic resonance
CC_{50}	50% Cytotoxic concentration
$CDCl_3$	Deuterated chloroform
CFU	Colony-forming unit

CHN	Carbon, hydrogen, nitrogen
CO_2	Carbon dioxide
COSY	Correlation spectroscopy
CvdW	Coulomb-van der Waals
d	Doublet
dd	Doublet of doublet
DEPT	Distortionless enhancement by polarization transfer
DMEM	Dulbecco's modified Eagle's medium
DMSO	Dimethyl sulfoxide
DOTS	Directly observed treatment, short-course
E. coli	*Escherichia coli*
EMB	Ethambutol
ESI-MS	Electronspray ionization mass spectrometry
FabI	Enoyl-ACP reductase
FAS	Fatty acid synthase
FCS	Foetal calf serum
FQ	Fluorescence-quenching intensity
FTIR	Fourier transform infrared spectroscopy
GScore	Glide score
GUI	Graphical user interface
h	Hour
^{1}H NMR	Proton nuclear magnetic resonance
HCl	Hydrochloric acid
HIV	Human immunodeficiency virus
HMBC	Heteronuclear multiple bond correlation

HMQC	Heteronuclear multiple quantum correlation
HPLC	High performance liquid chromatography
IC_{50}	Half maximal (50%) inhibitory concentration
IC_{90}	90% Inhibitory concentration
INH	Isoniazid
InhA	Enoyl-acyl carrier protein reductase from *Mycobacterium tuberculosis*
J	Coupling constant
K	Kelvin
KatG	Mycobacterial catalase-peroxidase hemoprotein
logPo/w	Logarithm of partition coefficient between octanol and water
m	Multiplet
MDCK	Madin-Darby canine kidney
MDR	Multiple drug resistant
Mg	Magnesium
MIC	Minimum inhibitory concentration
min	Minute
mL	Milliliter
mM	Millimolar
MS	Mass spectrometry
Mtb	*Mycobacterium tuberculosis*
MTS	3-(4,5-Dimethylthiazol-2-yl)-5-(3-carboxymethoxyphenyl)-2-(4-sulfophenyl)-2H-tetrazolium
MTT	3-(4,5-Dimethylthiazol-2-yl)-2,5-diphenyltetrazolium bromide
m/z	Mass-to-charge ratio

NA	Not available
NAD^+	Nicotinamide adenine dinucleotide (oxidized form)
NADH	Nicotinamide adenine dinucleotide (reduced form)
NaOH	Sodium hydroxide
ng/mL	Nanogram per milliliter
nm	Nanometer
nm/s	Nanometer per second
NMR	Nuclear magnetic resonance
OPLS	Optimized potentials for liquid simulation
ORTEP	Oak Ridge thermal ellipsoid plot
PDB	Protein data bank
PP_i	Pyrophosphate
ppm	Parts per million
PSA	Polar surface area
PZA	Pyrazinamide
R_f	Retention factor
RIF	Rifampicin
RMSD	Root-mean-square deviation
s	Singlet
S. Aures	*Staphylococcus aureus*
SAR	Structure-activity relationship
SI	Selectivity index
SOI	Secondary orbital interaction
t	Triplet
TAACF	Tuberculosis Antimicrobial Acquisition and Coordinating Facility

TB	Tuberculosis
TLC	Thin layer chromatography
TMS	Tetramethylsilane
TSA	Trypticase soy agar
UV	Ultraviolet
v/v	Volume per volume
WHO	World Health Organization
WST-1	4-[3-(4-Iodophenyl)-2-(4-nitrophenyl)-2*H*-5-tetrazolio]-1,3-benzene disulfonate
XDR	Extensively drug resistant
XP	Extra precision
XRD	X-ray diffraction
XTT	2,3-Bis-(2-methoxy-4-nitro-5-sulfophenyl)-2H-tetrazolium-5-carboxanilide

SINTESIS DAN KAJIAN AKTIVITI SEBATIAN-SEBATIAN NOVEL DISPIRO PIROLIDINA SEBAGAI AGEN ANTIMIKROBAKTERIAL BERPOTENSI

ABSTRAK

Sekumpulan dispiro pirolidina yang mengandungi lima puluh dua sebatian telah berjaya disintesis dengan menggunakan penambahan siklo 1,3 dwikutub. Tindak balas ini terbukti sangat regioselektif, menghasilkan satu set regioisomer sahaja sebagai produk. Sebatian-sebatian ini telah dikenalpasti melalui pelbagai kaedah instrumentasi seperti CHN, NMR, spektrometri jisim dan analisis sinar-X. Aktiviti anti-mikrobakteria bagi dispiro pirolidina yang baru disintesiskan telah diuji terhadap strain *Mycobacterium tuberculosis* $H_{37}R_V$ dengan mnggunakan asai “BacTiter-Glo Microbial Cell Viability”. Sebatian **3c**, atau 4´-(4-bromofenil)-1´-metilldispiro[asenaftalin-1,2´-pirolidina-3´,2″-indane]-2,1″(1*H*)-dion merupakan sebatian yang paling aktif, dengan IC_{50} pada 2.20 µM dan MIC pada 12.5 µM. Berbanding dengan drug-drug rujukan, sebatian **3c** adalah lebih aktif berbanding sikloserin dan pirimetamin, sebanyak 10.7-, 11.0-kali ganda bagi IC_{50} dan lebih daripada 8 ganda bagi MIC. Sebatian **3c** turut mempamerkan aktiviti yang setanding dengan etambutol tetapi kurang aktif berbanding isoniazid. Ujian sitoktosik telah dijalankan ke atas Hs27 dan fibroblas kolorektal primer untuk memeriksa toleransi sebatian-sebatian aktif ini terhadap sel-sel manusia. Sebatian utama **3c** dibuktikan tidak bertoksik sehingga 250 µM dan mencatatkan indeks pemilihan yang baik, iaitu >20. Analisis penambatan molekul telah dilakukan untuk memahami interaksi-interaksi yang penting antara sebatian yang aktif dengan sasaran enzim, iaitu protein

pembawa enoil-asil reduktase (InhA). Kumpulan sebatian ini didapati dicantumkan secara berkomputer pada tapak substrat, dan sebatian-sebatian ini menunjukkan potensi untuk bertanding dengan substrat asid lemak dan merencat enzim tersebut. Sebatian **3c** terutamanya, menunjukkan rangkaian ikatan hidrogen yang penting pada kdua-dua asid amino pemangkin Tyr 158 dan faktor pembawa nukelotida yang merupakan ciri terpelihara bagi perencat yang dikenalpasti setakat ini. Untuk menyokong kajian *in silico* ini, asai ikatan protein-ligan secara langsung telah digunakan dengan berdasarkan pendarfluor intrinsik triptofan daripada protein ini. Ikatan **3c** kepada InhA telah mengubahkan konformasi protein ini dan menyebabkan pelindapkejutan pendarfluor yang bergantung pada kepekatan dan masa. Dengan keperluan segera agen antituberkular baharu, kajian ini telah menunjukkan dispiro pirolidina merupakan sebatian pemula yang praktikal untul penemuan ubat-ubatan TB.

SYNTHESIS AND ACTIVITY STUDIES OF NOVEL DISPIRO PYRROLIDINE COMPOUNDS AS POTENTIAL ANTIMYCOBACTERIAL AGENTS

ABSTRACT

A mini library of fifty two highly functionalized dispiro pyrrolidines were synthesized successfully using 1,3-dipolar cycloaddition. This reaction is proved to be highly regioselective, giving only one set of regioisomer as product. These compounds were characterized using various instrumental methods such as CHN, NMR, mass spectrometry and X-ray analysis. The antimycobacterial activity of the newly synthesized dispiro pyrrolidines were tested against *Mycobacterium tuberculosis* $H_{37}R_V$ strains using BacTiter-Glo Microbial Cell Viability assay. Compound **3c**, or 4´-(4-bromophenyl)-1´-methyldispiro[acenaphthylene-1,2´-pyrrolidine-3´,2″-indane]-2,1″(1*H*)-dione was found to be the most potent among all, with IC_{50} of 2.20 µM and MIC of 12.5 µM. Comparing with standard drugs, compound **3c** was found to be more potent than cycloserine and pyrimethamine by 10.7-, 11.0-fold at IC_{50} and more than 8-fold at MIC. Compound **3c** also exerted a comparable activity with ethambutol but less potent when compared to isoniazid. Cytotoxicity study was performed using Hs27 and primary colorectal fibroblasts to screen the tolerability of the active compounds in human cells. The lead compound **3c** was proven to be non-toxic up to 250 µM and recorded a good selectivity index of >20. Molecular docking analysis was carried out to understand the important interactions of the active compounds with the target enzyme, enoyl-acyl carrier protein reductase (InhA). This class of compounds were found to dock at the

substrate binding site, which can potentially compete with the fatty acyl substrate and inhibit the enzyme. Compound **3c** especially, displayed the important dual hydrogen bonding network with catalytic residue Tyr 158 and the nucleotide cofactor, which is a conserved feature in most of the known inhibitors identified so far. To support the *in silico* study, direct protein-ligand binding assay was used based on the intrinsic tryptophan fluorescence of the protein. The binding of **3c** to InhA resulted in a conformational change of the protein, causing concentration- and time-dependent fluorescence quenching. With the urgent need of new antitubercular agents, these findings have established dispiro pyrrolidines as a practical lead for TB drug discovery.

CHAPTER ONE

INTRODUCTION

1.1 Tuberculosis

1.1.1 Overview

Tuberculosis (TB) remains one of the biggest public health problems in the 21st century. It ranks as the second leading cause of death from an infectious disease worldwide after AIDS. India and China have accounted for approximately 38% of the world's TB cases (World Health Organization, 2013). In spite of the availability of highly efficacious treatment for decades, one-third of the world's population still harbour a latent form of *Mycobacterium tuberculosis*, with the risk of reactivation of about 10% over the lifetime (Villemagne et al., 2012; Stead, 1967). The WHO report estimated almost 9 million cases and 1.5 million TB deaths in 2013, including 0.36 million people who were HIV-positive as well (World Health Organization, 2014a). In Malaysia, the current estimated incidence was 99 per 100,000 population, with the number of new TB cases increased from 15,000 in 2005 to 23,417 in 2013 (World Health Organization, 2015; Rashid Ali et al., 2015). For HIV patients with latent (or dormant) form of TB, the risk to develop active TB is higher due to the lack of immune capability to suppress the proliferation of the bacilli. Studies have found that HIV-positive patients are 20-30 times more likely to develop TB than HIV-negative individuals (Kwan and Ernst, 2011). To make matters worse, multiple drug resistant (MDR) and extensively drug resistant (XDR) strains of TB are on the rise (Gandhi et al., 2010). In 2013 there were an estimated of 480, 000 people who developed MDR-

TB, and 9% of them were diagnosed with XDR-TB as well. Globally there were total 100 countries that have been reported with XDR-TB cases (World Health Organization, 2014a). The emergence of these drug resistant strains as well as the co-infection of HIV have heightened the need for development of new drugs to combat this disease.

1.1.2 *Mycobacterium tuberculosis*

In 1882, Robert Koch identified *Mycobacterium tuberculosis* (*Mtb*) as the causative agent of TB. This Mycobacterium family has over 60 species, with only a few like *Mtb*, *Mycobacterium africanum*, *Mycobacterium bovis*, *Mycobacterium microti* and *Mycobacterium avium* that can lead to human diseases (Lawn and Zumla, 2011; Sarkar and Suresh, 2011). *Mtb* is an aerobic, non-encapsulated and non-motile rod-shaped bacterium. It grows most successfully in tissues with high oxygen content, and that is the reason why *Mtb* complexes are found mostly in the well-aerated upper lobes of lungs (Todar, 2009). Although *Mtb* contains peptidoglycan in its cell wall but it is neither classified as Gram-positive nor Gram-negative bacterium. This is due to the unusual, waxy coating on its cell surface that makes the cell impermeable to Gram staining. Instead, acid fast method is used to stain the bacterium since it resists decolourisation with acidified organic solvents once being stained (Lawn and Zumla, 2011).

The primary mode of transmission of *Mtb* is through air in aerosolized form. For example, inhalation of a few droplet nuclei of 2–5 µm containing as few as 1–3 bacilli will lead to TB infection (Koul et al., 2011). After inhaling, these bacilli are mainly engulfed by alveolar macrophages. The activated macrophages kill the bacteria by phagolysosomes whereas in naïve macrophages, phagosomes containing bacilli do not mature and will lead to primary infection (Deretic and Fratti, 1999). There are two possibilities at this stage in naïve macrophages: *Mtb* either multiplies intracellularly which leads to TB infection, or the bacteria are able to evade the host immune system and remain as dormant. The dormant stage will be reactivated into second infection when the host immunity is compromised (Sarkar and Suresh, 2011).

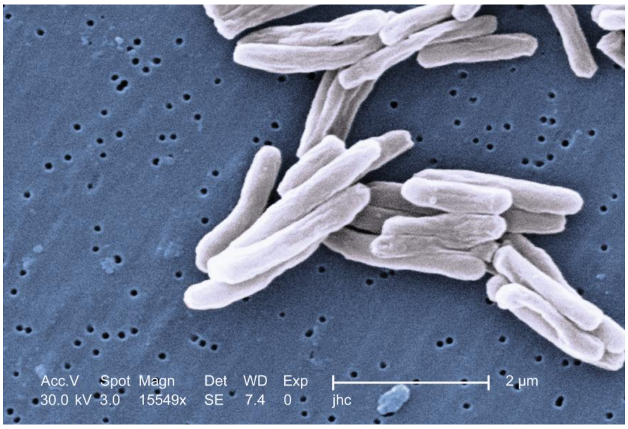

Figure 1.1 Scanning electron micrograph of *Mycobacterium tuberculosis* ranges in length between 2 - 4 microns, and a width between 0.2 - 0.5 microns (Adapted from Butler, 2006).

1.1.3 Current TB drug therapy

TB treatment is challenging and requires effective treatment regimens and follow-up support (Zumla et al., 2013). *Mtb* is a slow growing pathogen and thus administration of a combination of drugs for an extended period is required to achieve effective treatment and to prevent the emergence of drug-resistant strains (Craig, 1997). The history of first-line TB treatments began from monotherapy of streptomycin in 1946, and gradually evolved to multidrug treatment regimens of 24 months or more, until the current short course, directly observed therapy (DOTS) for at least 6 months (Fox et al., 1999; Wells et al., 2013). DOTS, is currently the best therapy program to treat TB patients, with cure rate of more than 95%. However DOTS alone is not efficient in areas with high incidence of drug-resistant strains, with cure rate of merely 50% (Zhang, 2005; Kimerling et al., 1999).

Current TB chemotherapy uses a combination of first-line drugs, starting with an intensive phase of 2 months of four drugs: isoniazid (INH), rifampicin (RIF), pyrazinamide (PZA) and ethambutol (EMB), followed by 4 months of continuation phase of INH and RIF (Blumberg et al., 2003). If the treatment fails in the case of bacterial drug resistance or intolerance of one of the first-line drugs, second-line drugs such as fluoroquinolones, cycloserine, kanamycin, para-aminosalicylate and ethionamide will be administered. These second-line drugs are usually more toxic, less effective and require longer duration of treatment than first-line drugs. Furthermore, some of these second-line drugs are not available in many poorer regions (van den Boogaard et al., 2009).

To gain insight into the mechanisms of the available TB drugs, a brief description of the first-line and second-line antitubercular agents are given as follow:

1.1.3(a) First-line TB drugs

(i) Isoniazid (INH)

Since its discovery in 1952, isoniazid (INH) (Figure 1.2) remains one of the most important first-line anti-TB drugs. It paved a major milestone in TB chemotherapy due to its high efficacy and mild side effects. More importantly, it is relatively inexpensive. INH shows high early bactericidal activity against rapidly dividing mycobacteria and kills about 95% of organisms in the first two days of treatment. However when the mycobacteria are in a slow or non-growing state, INH will become bacteristatic and is no more effective than other drugs at this period (Mitchison, 2000). INH is a prodrug that requires activation by catalase-peroxidase hemoprotein, KatG to produce a range of highly reactive species. These reactive oxygen species and organic radicals will then attack multiple targets in *Mtb* (Zhang, 2005). The primary target of activated INH is enoyl-acyl carrier protein reductase (or InhA), an essential enzyme in FAS II system which involves in mycolic acid synthesis (Banerjee et al., 1994). INH resistance is the most common form among anti-TB drugs, at the frequency of 1 in 10^{5-6} bacilli *in vitro* (Karakousis, 2009). Resistance mutations mostly happen in the target gene, InhA and in the activating enzyme, KatG (Global Alliance for TB Drug Development, 2008).

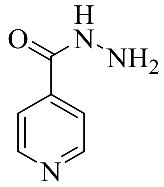

Figure 1.2 Chemical structure of isoniazid.

(ii) Rifampicin (RIF)

Rifampicin (RIF) or rifampin (Figure 1.3) is a broad-spectrum semisynthetic macrocyclic antibiotic produced by *Streptomyces mediterranei* (Craig, 1997). It was introduced in 1967 as a drug of choice for TB treatment. It is categorized as the bactericidal agent and is active against both replicating and non-replicating mycobacteria. The activity against the latter is thought to shorten the duration of TB therapy from 12-18 months to 9 months (Mitchison, 1985). RIF inhibits the bacterial RNA synthesis by binding to the β-subunit of the DNA-dependent RNA polymerase which is encoded by *rpoB* (McClure and Cech, 1978; Zhang, 2005). It does not inhibit mammalian enzymes. RIF-resistant *Mtb* involves alterations of RNA polymerase. There is approximately 96% of mutants occur in 81-bp region of *rpoB* gene, which is the RIF resistance-determining region (RDR) (Telenti et al., 1993).

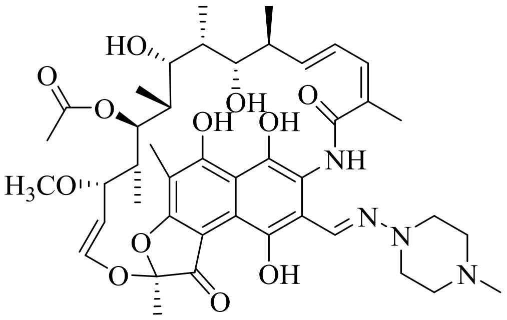

Figure 1.3 Chemical structure of rifampicin.

(iii) Pyrazinamide (PZA)

Pyrazinamide (PZA) (Figure 1.4) is a synthetic analogue of nicotinamide that was first chemically synthesized in 1936 by Dalmer and Walter. It appeared as a potential anti-TB drug in 1952 (Zhang and Mitchison, 2003). It has high *in vivo* sterilizing activity and represents the only first-line drug that kills the persisting tubercle bacilli. It is added to the initial intensive phase of chemotherapy and plays a role in reducing the treatment duration from 9 months to 6 months (Craig, 1997). The mechanism of action of PZA is the least poorly understood among all anti-TB drugs. PZA is a prodrug that requires activation by PZase/nicotinamidase enzyme (encoded by *pncA* gene) to form pyrazinoic acid (POA) (Scorpio and Zhang, 1996). POA that is formed initially in neutral cytoplasmic environment has no activity against mycobacteria. However under acidic conditions it is converted to uncharged protonated POA that permeates the cells through membrane, where it accumulates and kills the bacteria (Zhang and Mitchison, 2003). Mutation in *pncA* is a major mechanism of PZA resistance in *Mtb* (Marttila et al., 1999).

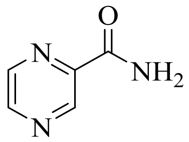

Figure 1.4 Chemical structure of pyrazinamide.

(iv) Ethambutol (EMB)

Ethambutol (EMB) (Figure 1.5) is a synthetic compound that was reported to show antimycobacterial activity in 1961 and has been prescribed in TB treatment since 1966. EMB is bacteriostatic against actively growing bacteria and it has been reported to inhibit several *Mtb* cellular pathways. The primary target of EMB is the biosynthesis of arabinogalactan, a major polysaccharide of mycobacterial cell wall (Takayama and Kilburn, 1989). It inhibits the polymerization of the arabinan component of arabinogalactan and of lipoarabinomannan, via inhibition of three arabinosyltransferases: *emb*A, *emb*B and *emb*C (Goude et al., 2009). Majority of the EMB-resistant clinical isolates relate to point mutations in *emb*B, with about 60% of the isolates carry a mutation in codon 306 (Sreevatsan et al., 1997; Plinke et al., 2006).

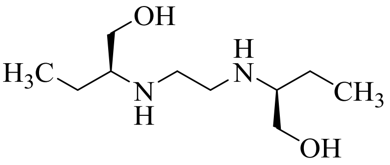

Figure 1.5 Chemical structure of ethambutol.

1.1.3(b) Second-line TB drugs

Second-line TB drugs (Figure 1.6) are considered as reserve therapy and are administered under special conditions such as the treatment of drug-resistant strains. *p*-Aminosalicylic acid represented one of the first TB antibiotics but its use as first-line regimen was discontinued after the discovery of drugs which are more potent such as RIF. It is still used as part of the treatment for XDR-TB although its mechanism of action has not been clearly elucidated (Jnawali and Ryoo, 2013). Aminoglycosides (such as amikacin and kanamycin) and cyclic polypeptides (such as capreomycin) are important injectable drugs used to treat MDR-TB by interfering with the protein synthesis of mycobacteria (Zhang, 2005). Fluoroquinolones (FQs) such as ciprofloxacin, ofloxacin and levofloxacin have broad-spectrum antimicrobial activity and are known as bactericidal antibiotics (Wang et al., 2006; Emmerson and Jones, 2003). FQs inhibit the DNA synthesis of *Mtb* by targeting DNA gyrase, the sole type II topoisomerase in mycobacteria (Aubry et al., 2004). Analogues of INH such as ethionamide and prothionamide are also prodrugs that require bioactivation by enzyme EthA. They inhibit the same target as INH, which is InhA gene (Banerjee et al., 1994). Cycloserine is an analogue of amino acid D-alanine that is recommended to treat MDR- and XDR-TB in the DOTS-Plus management plan (World Health Organization, 2011). It inhibits the synthesis of peptidoglycans which are essential in bacterial cell wall formation (Jnawali and Ryoo, 2013).

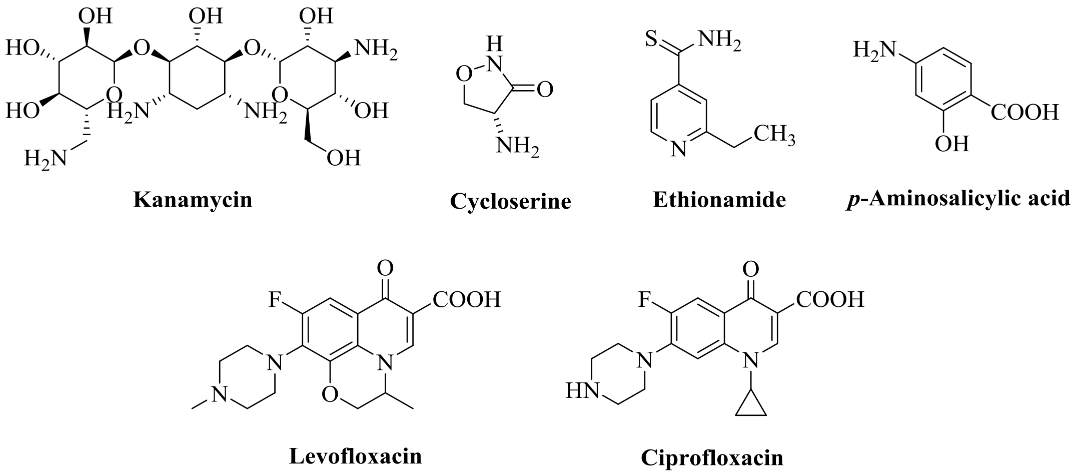
Kanamycin **Cycloserine** **Ethionamide** ***p*-Aminosalicylic acid**

Levofloxacin **Ciprofloxacin**

Figure 1.6 Structures of some second-line drugs for TB treatment.

1.1.4 Challenges in TB treatment

Although DOTS has proven to be highly efficient, the lengthy and complicated treatment makes patients compliance difficult. This noncompliance is the main reason that causes the development of drug-resistant strains, which poses a significant threat to the treatment and control of this disease (Zhang, 2005). MDR-TB are defined as strains that are resistant to first line drugs isoniazid (INH) and rifampicin (RIF); whereas XDR-TB are strains that are resistant not only to INH and RIF, but also to any fluoroquinolones and at least one of the three injectable second-line drugs: amikacin, kanamycin and capreomycin (Chiang et al., 2010). Currently MDR-TB is treated by a combination of a few drugs with duration of therapy for 18-24 months (Gandhi et al., 2010). This suboptimal therapy is less effective and causes approximately 30% of patients suffering from treatment failure (Mitnick et al., 2003). Treatment of XDR-TB is even more challenging. Only limited options of regimens can be used to treat XDR-TB since the bacilli are resistant to most of the available first-line and second-line drugs.

Starting from the 1980s, the growing pandemic of HIV/AIDS has fuelled a surge in TB cases globally, especially in the African region (World Health Organization, 2013). The frequent TB-HIV co-infection has further complicated the selection of an appropriate treatment. The main pharmacokinetic interaction between anti-TB agents and antiretrovirals is rifampicin induces a number of drug-metabolising enzymes, thus increases the expression of the hepatic cytochrome (CYP) P450 oxidase system (Niemi et al., 2003). This CYP induction leads to sub-therapeutic concentrations of many co-medications such as HIV protease inhibitors (Mallolas et al., 2007). Besides that, the overlapping toxic effects increase safety concerns for TB-HIV co-infected patients (Koul et al., 2011).

Furthermore, investment in TB drug research and development is insufficient relative to the burden of this disease. The 2013 Report on Tuberculosis Research Funding Trends, 2005-2012 revealed that the funding for TB R&D was cut by US$30.4 million in 2012 compared with the previous year (Frick and Jiménez-Levi, 2013). The private sector also reduced their funding by 22.1% (Burki, 2014). The pullout of major pharmaceutical companies such as Pfizer and AstraZeneca from this field in the past year brought a big impact to global TB research (Lessem, 2014). Pharmaceutical investments were likely to drop further in the next few years.

1.1.5 New drugs in pipeline

For the first time in nearly five decades, a promising TB drug pipeline has emerged. A number of new and repurposed therapeutic agents are under investigation and in phase I to phase III clinical trials (Lienhardt et al., 2012). These include novel chemical entities as well as the known drugs that are used to treat other diseases. By combining the new candidates with the existing TB drugs it is hoped that the treatment duration can be reduced and TB drug-resistant strains can be cured.

The Global Alliance for TB Drug Development is currently evaluating the feasibility of a fluoroquinolone-based regimen to reduce the treatment duration of drug-susceptible TB from 6 months to 4 months (Burki, 2014). Later-generation of fluoroquinolones such as gatifloxacin and moxifloxacin (Figure 1.7) have been proved to possess high efficacy and safety in MDR-TB treatment (Kwon et al., 2014). Rifapentine (Figure 1.7) has been tested in a combination with isoniazid at phase III clinical trial. However this regimen showed high failure rates in HIV-positive patients as well as those with cavitary pulmonary TB (Benator et al., 2002). Linezolid (Figure 1.7), a first generation of oxazolidinone in phase II, has the potential to treat MDR/XDR-TB, but its significant toxicity limits its long-term use (Kwon et al., 2014).

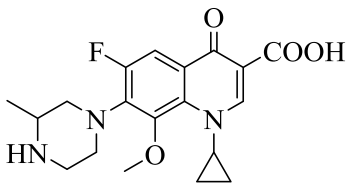

Gatifloxacin

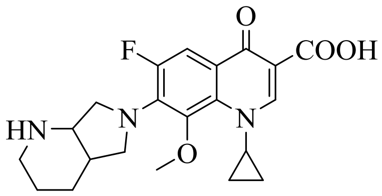

Motifloxacin

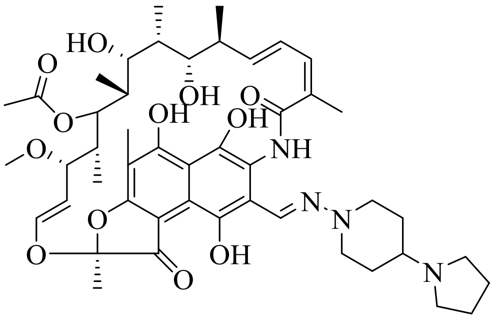

Rifapentine

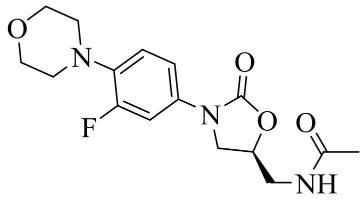

Linezolid

Figure 1.7 Chemical structures of potential TB drugs in clinical development.

Bedaquiline (Figure 1.8) represents the first antitubercular drug to be approved for the past 40 years after rifampicin. It inhibits mycobacterial adenosine triphosphate (ATP) synthase, a key enzyme in the energy metabolism of *Mtb* (Haagsma et al., 2011). It was granted accelerated approval by the US Food and Drug Administration (FDA) in 2012 as part of the treatment regimen for MDR-TB based on limited efficacy and safety data from Phase II studies (Chan et al., 2013). Therefore WHO issued “interim policy guideline” for the usage of bedaquiline when other treatment alternatives are not available (World Health Organization, 2013).

Delamanid (Figure 1.8), a novel nitroimidazole-oxazole derivative, is the second new drug to receive regulatory approval by the European Medicine Agency in 2014. It is suggested by WHO as an interim recommendation to treat adults with MDR-TB under conditions when an effective treatment regimen is unavailable (World Health Organization, 2014b). It is a prodrug that blocks the biosynthesis of mycolic acids in

Mtb and thus disrupts its cell wall (Zumla et al., 2013). This new drug has only been through Phase IIb clinical trial and is currently in pediatrics and Phase III trials (Lessem, 2014).

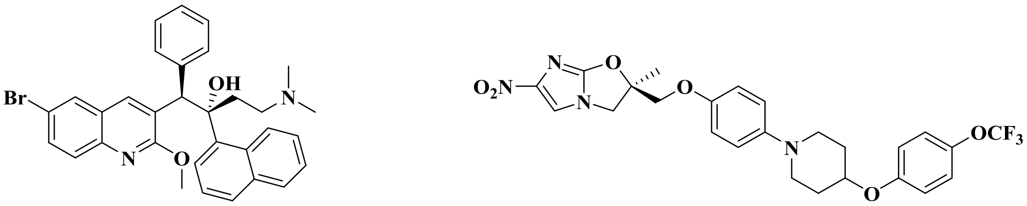

TMC 207 (bedaquiline) **OPC 67683 (delamanid)**

Figure 1.8 Newly approved drugs for treatment of MDR-TB under “interim policy guideline”.

1.1.6 Potential drug targets

Advancements in molecular biology and the development of powerful genetic tools have accelerated the rate in discovery of new therapeutic targets. Transposon mutagenesis, gene knockout and gene transfer methods have been used recently to identify genes that are essential for the survival of *Mtb in vitro* and *in vivo* (Zhang et al., 2006; Lamichhane et al., 2003). New drugs should be targeting not only on the metabolically active *Mtb* but also to kill the persisters or non-growing bacilli (Lamichhane, 2011). Several pathways have been characterized as potential drug targets, including cell wall synthesis, energy metabolism pathways and protein processing (Zhang, 2005). Genes involved in the mycobacterial persistence, such as isocitrate lyase (Sharma et al., 2000), L,D-transpeptidase (Lavollay et al., 2008) and DosR (regulator involved in mycobacterial survival under hypoxic conditions (Park et al., 2003)), have also been identified as potential targets for new drug development.

Figure 1.9 represents a number of targets inhibited by the existing TB drugs as well as some potential new targets.

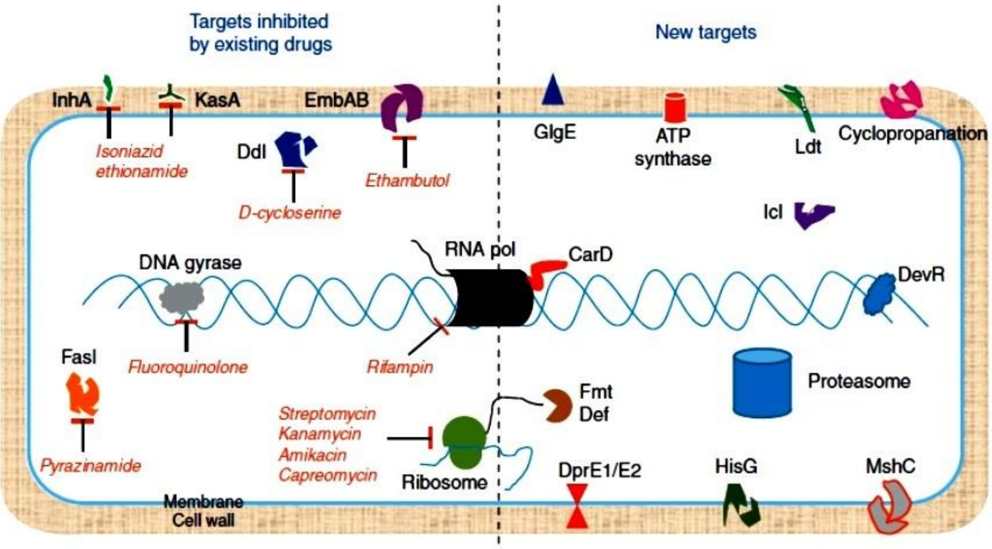
Targets inhibited by existing drugs
New targets
InhA
KasA
EmbAB
Isoniazid ethionamide
DdI
D-cycloserine
Ethambutol
GlgE
ATP synthase
Ldt
Cyclopropanation
Icl
DNA gyrase
RNA pol
CarD
DevR
FasI
Fluoroquinolone
Rifampin
Fmt
Def
Proteasome
Pyrazinamide
Streptomycin
Kanamycin
Amikacin
Capreomycin
Ribosome
DprE1/E2
HisG
MshC
Membrane
Cell wall

Figure 1.9 Targets implicated in TB disease (Adapted from Lamichhane, 2011).

Mtb has a unique cell wall that contributes to its pathogenicity (Tonge, 2000). It contains a very thick waxy, complex lipid-rich membrane which is highly hydrophobic and impermeable, thus helps the bacteria to persist and resistant to many chemotherapies (Barry III et al., 1998). Mycobacterial cell wall is composed of three covalently linked macromolecules: mycolic acids, peptidoglycan, and arabinogalactan. Till date, anti-TB drugs that are currently used include inhibitors of mycolic acids (isoniazid and ethionamide), arabinogalactan (ethambutol) and peptidoglycan (cycloserine) (Mdluli and Spigelman, 2006).

Mycolic acids are α-alkyl, β-hydroxy branched long chain fatty acids that form the protective layer of the cell envelope. To generate these long chain fatty acids, *Mtb* contains both FAS I and FAS II fatty acid biosynthesis systems (de Souza et al., 2008). FAS I is responsible for the *de novo* synthesis of C16-C26 fatty acids; and FAS II elongates these fatty acids up to C56 to produce precursors of mycolic acids (Mdluli and Spigelman, 2006). Enoyl-ACP reductase, encoded by InhA gene, is essential in the last step of elongation cycle in FAS II (Figure 1.10). It catalysed the NADH-specific reduction of 2-trans-enoyl ACP (Quemard et al., 1995).

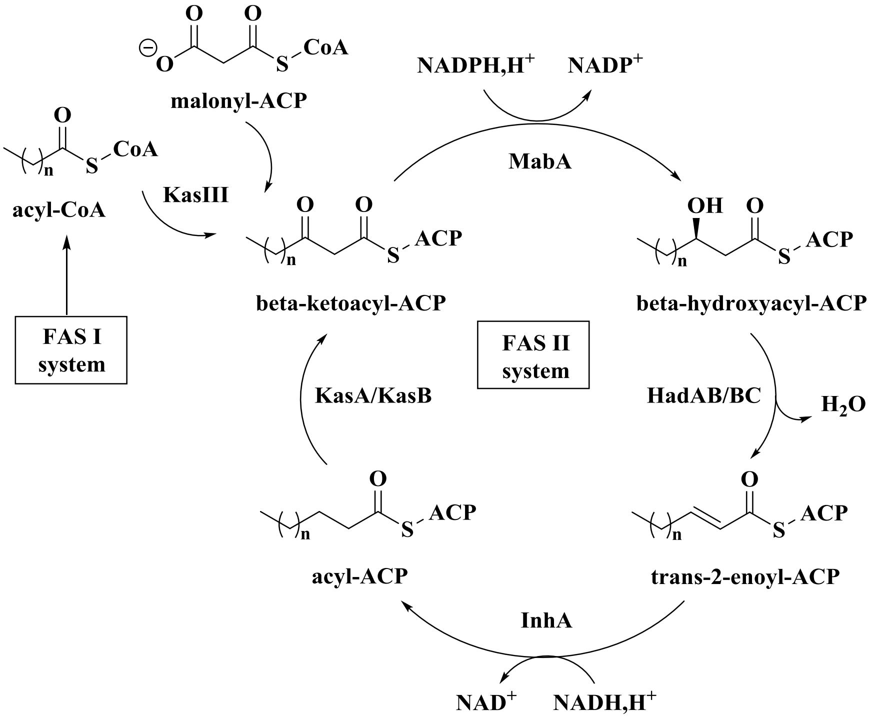
malonyl-ACP
acyl-CoA
KasIII
NADPH,H+
NADP+
MabA
beta-ketoacyl-ACP
beta-hydroxyacyl-ACP
FAS I system
FAS II system
KasA/KasB
HadAB/BC
H2O
acyl-ACP
trans-2-enoyl-ACP
InhA
NAD+
NADH,H+
CoA
ACP

Figure 1.10 FAS II system in *Mycobacterium tuberculosis*.

InhA belongs to the short-chain alcohol dehydrogenase/reductase (SDR) superfamily, characterized by their catalytic residues tyrosine 158 and lysine 165 (Parikh et al., 1999). It is now well established that InhA is the primary target of isoniazid (INH), one of the most powerful front-line drug for TB treatment. As a prodrug, INH does not inhibit InhA directly but must be activated by KatG to form the reactive acyl radical. The acyl radical then binds to the position 4 of nicotinamide adenine dinucleotide (NAD) to form an active INH-NAD adduct (Zhao et al., 2006). Clinical studies showed that high levels of resistance to INH are caused by mutations in KatG (Zhao et al., 2006; Suarez et al., 2009). Therefore inhibitors targeting InhA directly without the need of activation would be the promising candidates to develop new anti-TB drugs.

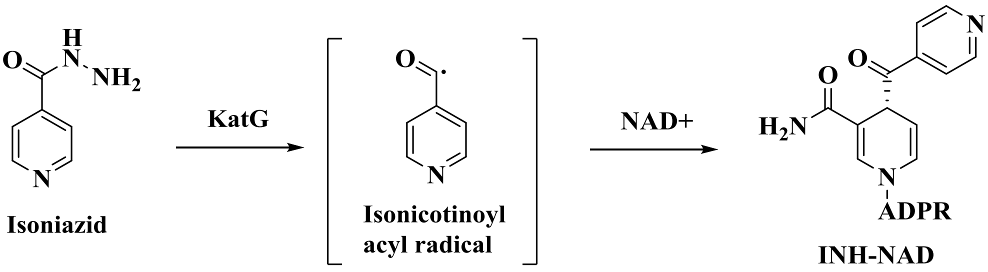

Figure 1.11 Activation of isoniazid (INH) by KatG to form INH-NAD adduct that inhibits InhA enzyme.

1.2 Drug design

1.2.1 Overview

Drugs are defined as chemical substances that are used to prevent and treat diseases (Thomas, 2004). Since human life is constantly threatened by many illnesses, it is of utmost importance to discover ideal drugs that can benefit humanity. The process of drug design and development is challenging, costly and time consuming. It starts from identification of a disease and its target, followed by lead discovery and optimization, *in vitro* and animal test, clinical studies in human beings, and finally to the regulatory approval and production (Figure 1.12). The average time to bring a new drug from research lab to patients is 10-15 years and the estimated cost is 1.3 billion US dollars (Turner, 2010). In 2013, 27 new molecular entities have been approved by FDA’s center for Drug Evaluation and Research (CDER) as novel new drugs (US Food and Drug Administration, 2014).

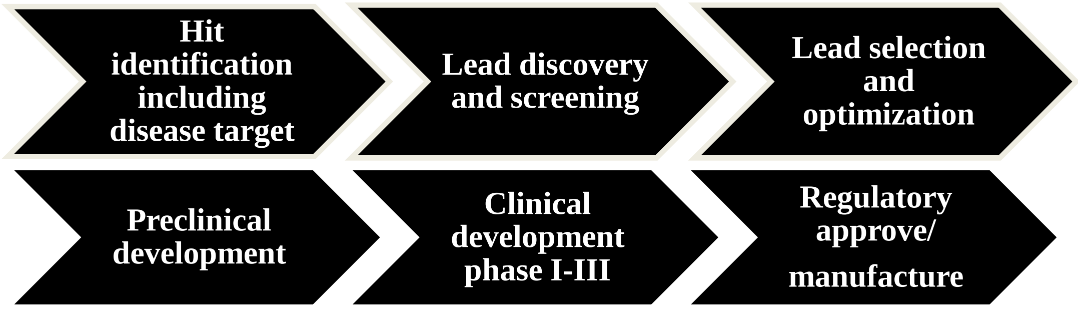
Hit identification including disease target
Lead discovery and screening
Lead selection and optimization
Preclinical development
Clinical development phase I-III
Regulatory approve/ manufacture

Figure 1.12 Process of drug discovery and development (Modified from *Nature Reviews Drug Discovery* (Wenk, 2005, Cooper, 2002)).

The whole process of drug development requires input from various fields, including medicinal chemistry, biology, pharmacology, biochemistry and computational chemistry (Thomas, 2004). The primary roles of medicinal chemists are to design and synthesize new compounds that are deemed suitable for use as drugs, followed by biological evaluation and generation of a new hypothesis to further improve the design and synthesis (Lowe, 2006). Methods like addition of functional groups, extension of structures, changing the type of substituent as well as its position, etc. are the common strategies used in drug design. The biological activity of a compound might be varied even with a slight change in the molecular structure. For example, by changing the ether linkage $-OCH_2-$ of the beta blocker propranolol to $-SCH_2-$, the activity will be diminished (Patrick, 1995). Therefore chemists usually synthesize a series of analogues, evaluate their biological activity and correlate the chemical structures with the optimum activity.

With the greater advancement and understanding of biochemical structures and physiological mechanisms, drugs can be designed using a “rational approach” (Pandeya and Dimmock, 1997). This approach takes into account the targets or sites of drug action so that drugs can be designed accordingly. The first rational development of synthetic drugs was started by Paul Ehrlich and Sacachiro Hata in 1910. They produced the antiprotozoal arshemamine by combining synthesis with reliable biological screening and evaluation procedures (Thomas, 2004). Today, rational drug design can be organized into four areas: pharmacophore-based and structure-based approaches which depend on whether the three-dimensional structure of the protein target is known; new lead generation and structure evaluation which can be performed regardless of the availability of the biological target structure (Reddy and Parrill Abby, 1999). This is where the analysis of structure-activity relationship (SAR), quantitative structure-activity relationship (QSAR), *de novo* design and combinatorial chemistry come in place.

Drug design and development is a multi-disciplinary field that requires scientists from different areas to work together to construct a virtual drug with desired chemical, biological and physical properties (Neamati and Barchi, 2002). In this postgenomic era, numerous novel and exciting techniques in proteomics, bioinformatics and genomic sequencing have been developed and implemented in the process of drug discovery for the past 5-10 years. Academic, healthcare, government and industrial sectors should collaborate and work hand in hand to drive the advancements from genetic and biological research into medical and commercial benefits for society (Hoelder et al., 2012).

1.2.2 Green chemistry in drug discovery

The term “green chemistry” is defined as the design of chemical products and processes that minimize or eliminate the use and production of hazardous substances (Anastas and Kirchhoff, 2002). It was conceptualised by Paul T. Anastas of the US Environmental Protection Agency (EPA) in 1993. Since then the field of green chemistry has been incorporated into many key research areas including catalysis, design of environmentally benign solvents, development of renewable feedstocks, usage of safer chemicals etc (Anastas and Kirchhoff, 2002). Twelve principles of green chemistry have been developed to provide a guideline of what would make a greener process, product or system (Anastas and Warner, 2000).

Chemical reactions play an important role in drug synthesis. Many of the traditional synthetic methods have broad scope but at the same time produce massive amounts of waste. The pharmaceutical industry has made significant efforts to minimize the usage of hazardous solvents and to reuse the catalysts to improve atom economy and environmental safety (Smita and Falguni, 2012). One of the most classical examples of how green chemistry can be applied in drug synthesis is the production of ibuprofen (Sheldon, 2010). As shown in Figure 1.13, the conventional method required a 6-step procedure with stoichiometric reagents, low atom efficiency, and production of secondary by-products and waste. In contrast, the green alternative developed in 1990s involved only three catalytic steps with increased efficiency and sustainability (Elango et al., 1991; Poliakoff and Licence, 2007). Most of the atoms of the reactants are incorporated into the desired product and unwanted by-products are reduced up to ten times.

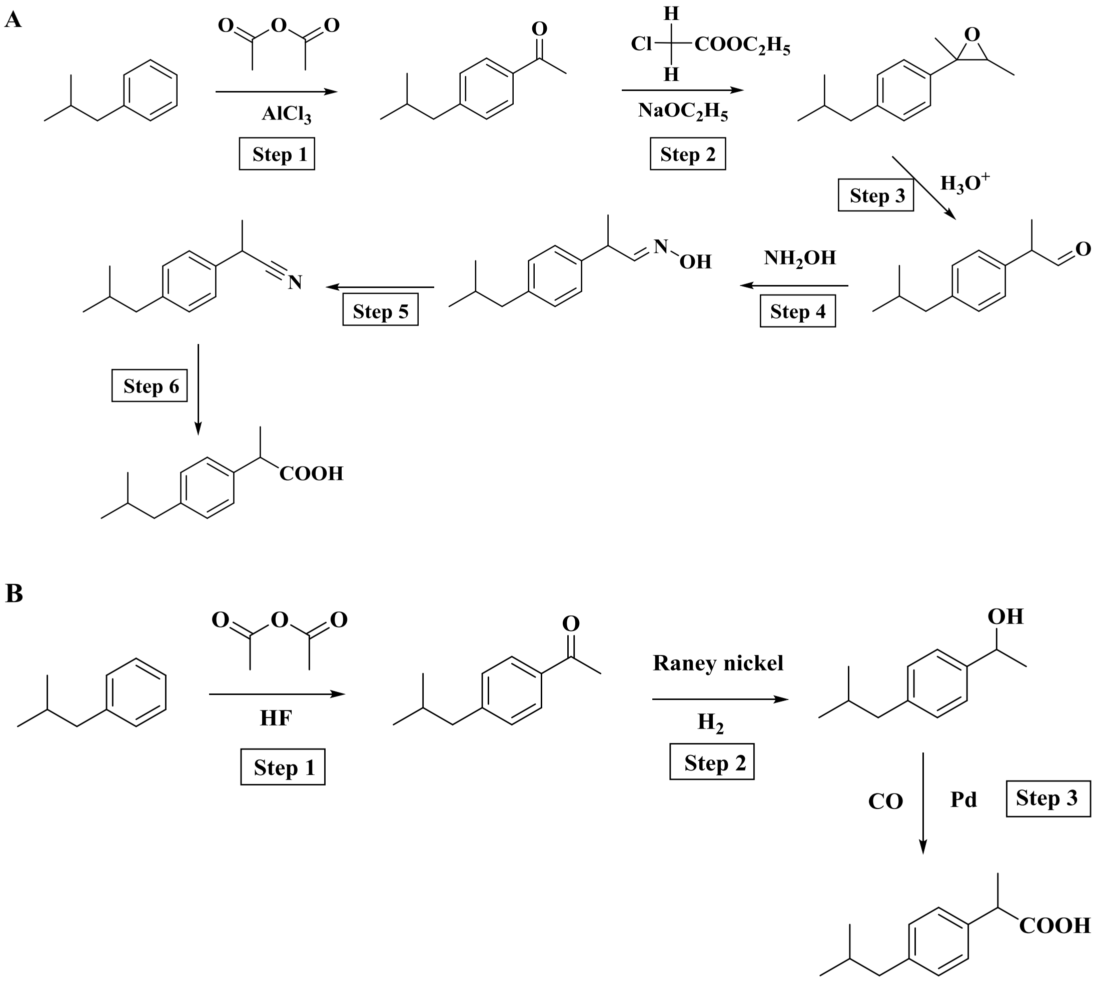
A
AlCl3
Step 1
Cl COOC2H5
NaOC2H5
Step 2
Step 3
H3O+
NH2OH
Step 4
Step 5
Step 6
N
OH
O
COOH
B
HF
Step 1
Raney nickel
H2
Step 2
OH
CO
Pd
Step 3
COOH

Figure 1.13 Synthesis of ibuprofen by using conventional six-step method (A) and the green synthesis that was reduced to three steps (B).

Researchers and pharmaceutical companies should be encouraged to utilize green chemistry procedures in drug discovery. Green solvents including water, liquid polymers, ionic liquids and supercritical fluids have great potential to contribute to more sustainable process (Leitner, 2009). Appropriate catalysts such as zeolites and montmorillonite clay are reusable, economically favourable and more environmental friendly (Kaneda et al., 2002). Some “green” reactions such as solvent-free microwave-assisted synthesis, grinding method and multicomponent one-pot reactions are also been used and promoted.

1.2.3 1,3-dipolar cycloaddition

In modern drug design, chemists are constantly working on to discover new and improved reactions to explore novel pharmacological agents. One of the major challenges of this research is the development of new transformations that are not only efficient, selective and high yield but also environmental friendly (Hazra et al., 2013). Tandem reactions, or sometimes known as domino, cascade, consecutive, iterative or one-pot reactions, link several transformations together in a single synthetic step (Bunce, 1995). Over the past decade, tandem reactions are of immense importance because they increase the synthetic efficacy to construct complex organic molecules without the needs to isolate and purify the intermediates. This helps in substantial minimization of waste, time, cost and labour (Li et al., 2008). Therefore it can be considered as a form of “green chemistry” (Li et al., 2008; Nicolaou et al., 2006).

1,3-dipolar cycloaddition, also known as the Huisgen cycloaddition, is a classical tandem reaction in organic chemistry. It consists of the reactions of 1,3-dipoles with olefinic or acetylenic dipolarophiles to construct various highly substituted five-membered rings in a regio- and stereoselective manner (Tsuge and Kanemasa, 1989; Manian et al., 2006). 1,3-dipole is a species that is represented by zwitterionic octet structure where the central atom must have an electron pair to stabilize the species by dispersal of the positive charge (Padwa, 1984). Dipolarophiles, on the other hand, are compounds that react with 1,3-dipole and they are typically alkenes or alkynes. The history of 1,3-dipoles traces back to 1883 when Theodor Curtius discovered diazoacetic ester. However it was only generalized in 1960s when Rolf Huisgen first established its synthetic application through systematic studies (Padwa, 1984). Today this reaction is widely practised in many areas, from material chemistry (Lutz, 2007), bioconjugation (Dirks et al., 2009), nanotechnology (Zhou et al., 2008) to drug discovery (Najera and Sansano, 2009).

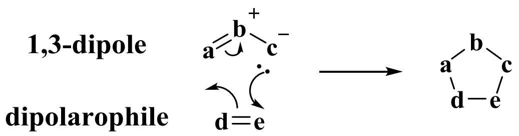

Figure 1.14 General scheme of 1,3-dipolar cycloaddition.

There are two types of mechanisms in 1,3-dipolar cycloaddition: concerted and step-wise. These mechanisms had been controversially debated in the late 1960s by Huisgen (Huisgen, 1968) and Firestone (Firestone, 1968). The concerted mechanism which was postulated by Huisgen, is thermally allowed with [$\pi 4_s + \pi 2_s$] according to the Woodward-Hoffmann rules. This involves 4 π electrons from the dipole and 2 π electrons from the dipolarophile. Three pz orbitals of the 1,3-dipole and two pz orbitals of the dipolarophile will combine suprafacially, and the stereochemistry of the reactants could then be transferred to the product. (Gothelf and Jørgensen, 1998). Step-wise biradical mechanism that was suggested by Firestone involved a two-step reaction with a discrete intermediate, a spin-paired diradical. The stereochemical information was thus destroyed during these transformations (Firestone, 1968). However this free radical mechanism was overwhelmed by the concerted mechanism and is no longer in favour (Quin and Tyrell, 2010).

The simple and easy accessible procedures of 1,3-dipolar cycloaddition reaction makes it a useful tool in constructing biologicaly important nitrogen-containing five-membered heterocycles such as pyrrolidines, oxindoles and isoxazolines (Figure 1.15). Fokas et al. (1998) reported the formation of spiro[pyrrolidine/oxindole] ring system through three component 1,3-dipolar cycloaddition using isatin, α-amino acids and chalcones. Dürüst et al. (2011) reported the regioselective 1,3-dipolar cycloaddition of phenanthrolinium ylides with (*Z*)-arylidene oxazolones. Xiao et al. (2013) also successfully synthesized the novel dispirooxindole, pyrrolo(spiro-[2.3′]-oxindole)-spiro-[4.3″]-oxindole via this reaction. All of these examples were depicted in Figure 1.16.

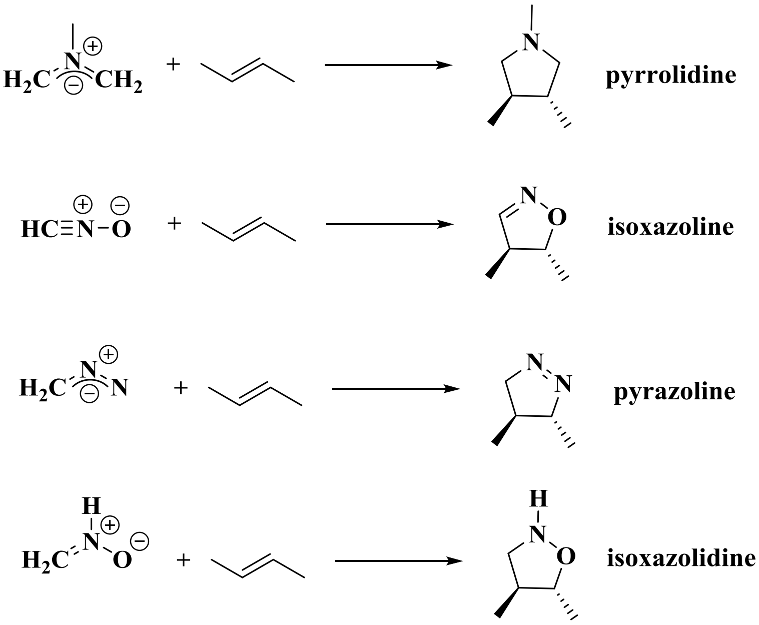

Figure 1.15 Examples of 1,3-dipolar cycloadditions in constructing various types of 5-membered heterocyclic compounds.

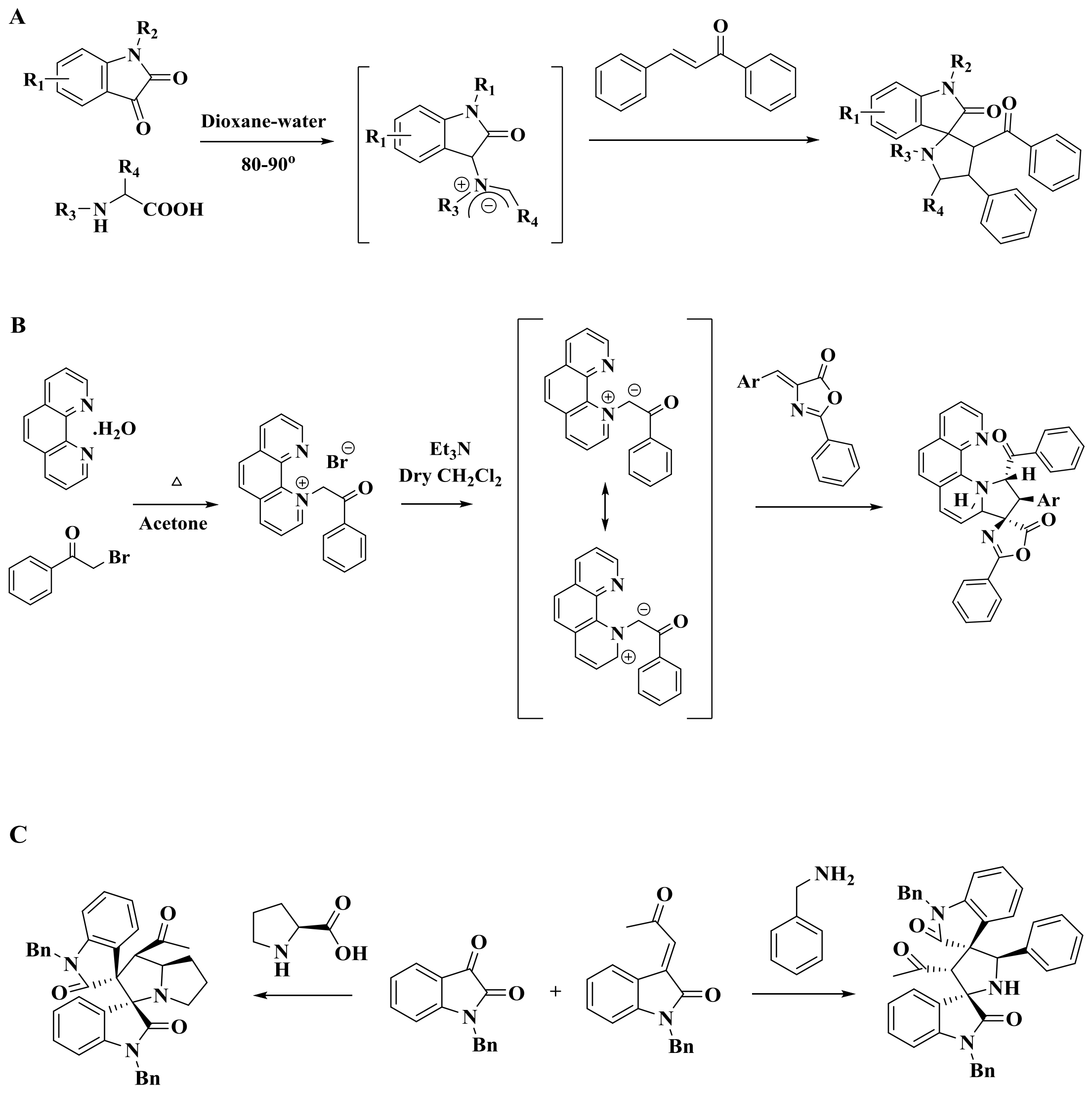
A
R2
R1
N
O
O
R4
R3
N
H
COOH
Dioxane-water
80-90°
R1
R1
R3
R4
R2
B
.H2O
N
N
△
Acetone
O
Br
Br
Et3N
Dry CH2Cl2
Ar
O
N
O
H
H
Ar
C
Bn
NH2
OH
NH
+
Bn

Figure 1.16 Known synthetic routes of different cycloadducts that have been published previously (Fokas et al, 1998; Dürüst et al., 2011; Xiao et al.).

1.2.4 Molecular docking in drug design

Molecular docking is an essential tool in structural molecular biology and computer-aided drug design (Morris and Lim-Wilby, 2008). It plays an important role in understanding drug-receptor interactions. The first docking algorithm for small molecules was developed in 1982 by the Kuntz group from University of California, San Francisco (Kuntz et al., 1982). Today, the increased availability of three